

# Surface Plasmon Polariton Amplification upon Electrical Injection in Highly Integrated Plasmonic Circuits

Dmitry Yu. Fedyanin,<sup>\*,†</sup> Alexey V. Krasavin,<sup>‡</sup> Aleksey V. Arsenin,<sup>†</sup> and Anatoly V. Zayats<sup>‡</sup>

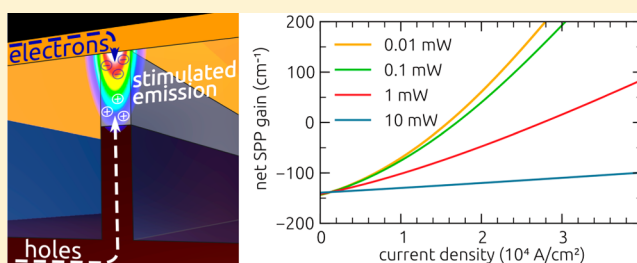
<sup>†</sup>Laboratory of Nanooptics and Femtosecond Electronics, Department of General Physics, Moscow Institute of Physics and Technology (State University), 9 Institutsky Lane, Dolgoprudny 141700, Russian Federation

<sup>‡</sup>Nano-optics and Near-field Spectroscopy Group, Department of Physics, King's College London, Strand, London WC2R 2LS, United Kingdom

## Supporting Information

**ABSTRACT:** We propose a very efficient approach for amplification of surface plasmon polaritons (SPPs) in a nanoscale waveguiding geometry with strong ( $\sim\lambda/10$ ) mode confinement. The implemented scheme of electric pumping is based on a single-heterostructure Schottky-barrier diode and has been numerically shown to ensure full compensation of the SPP propagation losses at wavelengths around  $3\ \mu\text{m}$  and, moreover, to provide net SPP gain. The presented concept creates the backbone for the implementation of highly integrated large-scale hybrid electronic-plasmonic circuits operating at extremely high speeds and opens the prospects for the realization of integrated coherent SPP sources.

**KEYWORDS:** Active plasmonics, optical amplifier, Schottky barrier diode, optical integrated circuits, optical interconnects



High heat generation in modern integrated circuits and problems with heat removal limit the increase of the clock rate in modern electronic microprocessors. Multicore architecture has been introduced to maintain the growth of the performance of single-chip integrated circuits without increasing the operation frequency. For example, modern graphics processor units contain more than 1000 stream processing units (i.e., cores); their performance exceeds 1 TFLOPS and is determined mainly by the bandwidth of interconnects rather than by the clock rate of the individual core, which is only about 1 GHz. Nevertheless, the bandwidth of conventional electrical on-chip interconnects is limited by the RC rise time and does not satisfy the requirements of modern and future multicore architectures.<sup>1</sup> Optical guides having ultrahigh bandwidth offer a promising alternative to electrical ones. But the transverse size of photonic waveguides is limited by diffraction and is much larger than the size of on-chip electronic components, as is the bending radius. Implementation of surface plasmon polariton (SPP) waveguides could solve this problem and move the dimensions of on-chip optical components closer to that of electronic ones.<sup>2,3</sup> However, SPPs suffer high propagation losses, since a significant amount of the SPP field is concentrated in the metal. One can decrease the portion of the SPP field in the metal by designing waveguiding geometries, where the plasmonic mode is located predominantly in the surrounding dielectric,<sup>4</sup> but doing this one also impairs the confinement so that it becomes worse than the confinement of light in photonic waveguides, which are free of ohmic losses. Over recent years, it has become clear that the only promising way to overcome propagation losses at the

nanoscale is to compensate losses in the metal. In this Letter, using a comprehensive hybrid electronic/photonic model, we demonstrate a novel type of nanoscale active plasmonic waveguides with integrated electric pumping that ensures lossless SPP guiding and, moreover, net SPP amplification.

Compensation of ohmic losses is possible through replacing the passive dielectric component near the metal surface with an active gain medium, which, under pumping, can amplify SPPs via stimulated emission. Several approaches to realize this concept have been demonstrated using optically pumped gain media based on dye molecules,<sup>5</sup> quantum dots,<sup>6,7</sup> fluorescent-conjugated polymers,<sup>8</sup> and semiconductors.<sup>9,10</sup> However, optical pumping requires the use of external high-power bulky pump lasers and is not feasible in ultracompact on-chip optical circuits. From this perspective, compact electric pumping is much more favorable.<sup>11</sup> The recently proposed approach based on a Schottky barrier diode<sup>12,13</sup> is very promising due to its simplicity (one needs only a metal-semiconductor Schottky contact to implement electric pumping) and relatively small value of the threshold current. However, an appropriate waveguiding geometry should be designed to realize this idea in a highly integrated plasmonic circuit. To achieve this, the following requirement should be taken into account: (1) back contact is needed to realize electric pumping; (2) planar configuration is required for effective and low-cost on-chip integration; (3) single-mode

**Received:** February 8, 2012

**Revised:** March 21, 2012

**Published:** March 26, 2012

guiding is much preferred; (4) bandwidth at least of the order of 100 Gbit/s is needed for competitive on-chip interconnects; and (5) high integration density of the plasmonic circuit is essential.

Among numerous plasmonic waveguide geometries, the T-shaped active plasmonic waveguide shown in Figure 1a

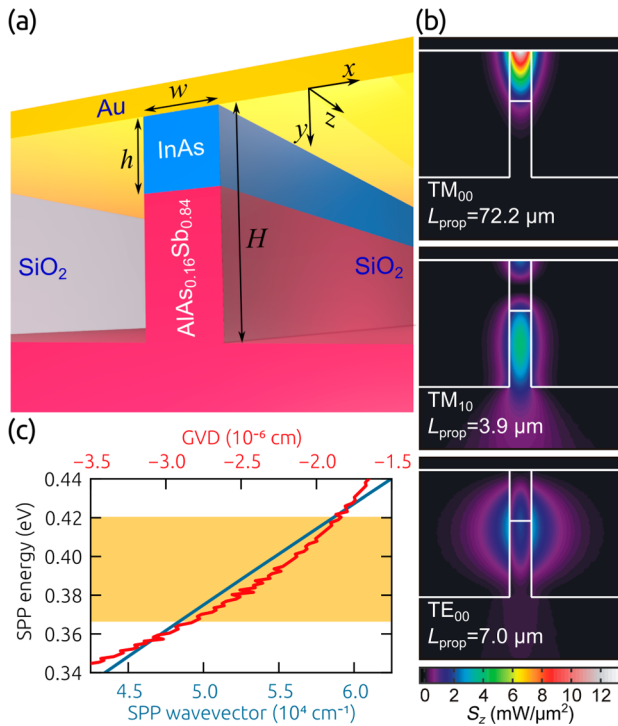


**Figure 1.** (a) Sketch of a T-shaped active plasmonic waveguide, which consists of the active p-type InAs layer with an acceptor concentration of  $2.33 \times 10^{18} \text{ cm}^{-3}$  and the passive p-type  $\text{AlAs}_{0.16}\text{Sb}_{0.84}$  layer with an acceptor concentration of  $2.0 \times 10^{18} \text{ cm}^{-3}$ ,  $w$  and  $H$  are the width and the height of the waveguide,  $h$  is the height of the InAs region. (b) Power flow maps for the modes of the T-shaped waveguide ( $w = 350 \text{ nm}$ ,  $H = 2 \mu\text{m}$  and  $h = 0.8 \mu\text{m}$ ) at an SPP energy of  $392.5 \text{ meV}$  ( $\lambda = 3.16 \mu\text{m}$ ), which corresponds to the maximum gain in InAs.<sup>13</sup>  $L_{\text{prop}}$  denotes the propagation length. All modes are normalized to carry the same power of  $1 \text{ mW}$ . The optical constants are set to  $\epsilon_{\text{Au}} = -521 + 36i$  (see Supporting Information),  $\epsilon_{\text{SiO}_2} = 2.00$ ,<sup>14</sup>  $\epsilon_{\text{InAs}} = 12.38$ ,<sup>15</sup>  $\epsilon_{\text{AlAs}_{0.16}\text{Sb}_{0.84}} = 10.18$ ;<sup>15</sup> we neglect free-carrier and band-to-band absorption in the semiconductors, since their contributions to the imaginary part of the SPP wavevector are only about 2 and  $3 \text{ cm}^{-1}$ , respectively; band-to-band transitions will be considered in the analysis of the SPP amplification. (c) Dispersion and group velocity dispersion (GVD) of the  $\text{TM}_{00}$  mode for the T-shaped waveguide considered in panel (b), yellow stripe indicates the gain bandwidth of InAs.<sup>13</sup>

favorably satisfies all the above requirements. In this waveguide, the SPP-supporting interface is formed by an active InAs layer used for SPP amplification and a metal superstrate, which also produces a Schottky contact for creation of the population inversion upon electrical injection. The  $\text{AlAs}_{0.16}\text{Sb}_{0.84}$  layer lattice-matched to InAs completes the SPP waveguide and acts as a back electrical contact to the active InAs layer. Finally, the waveguiding channel is surrounded by a low refractive index material ( $\text{SiO}_2$ ). To reveal the structure of the guided modes, eigenmode finite element numerical simulations have been performed at wavelengths around  $\lambda \sim 3 \mu\text{m}$ , corresponding to the gain spectral region in InAs.<sup>13</sup> The width of the

semiconductor core is chosen to be  $w = 350 \text{ nm}$  ( $\sim \lambda/10$ ) for the waveguide to support only modes with a single maximum in the  $x$ -direction and the main plasmonic  $\text{TM}_{00}$  mode (which has the same nature as the plasmonic mode in dielectric loaded SPP waveguides)<sup>6</sup> with a quite high effective index of 2.68 at  $\lambda = 3.16 \mu\text{m}$ . The waveguide height is set to be sufficiently large ( $H = 2 \mu\text{m}$ ) so that the plasmonic  $\text{TM}_{00}$  mode can be considered for on-chip data communication ( $L_{\text{prop}} = 72 \mu\text{m}$ ) but small enough so that the other supported modes ( $\text{TE}_{00}$  and  $\text{TM}_{10}$ ) are extremely leaky with more than ten times shorter propagation lengths ( $7.0$  and  $3.9 \mu\text{m}$  for the  $\text{TE}_{00}$  and  $\text{TM}_{10}$ , respectively) and have much more poor field localization (Figure 1b). Thus, a quasi-single-mode regime is realized. Moreover, for  $h < H/2$ , only the plasmonic  $\text{TM}_{00}$  mode is localized in the active InAs region, which will give it an additional advantage in terms of amplification.

SPP amplification upon electrical injection is a complex phenomenon involving both electrical and optical processes, the latter being specific to its plasmonic nature. From the electronic point of view, Au/p-InAs interface is a Schottky contact. At a temperature of  $77 \text{ K}$ , which is chosen due to the relatively small bandgap energy  $E_g^{\text{InAs}}$  of InAs and is typical for mid-infrared optoelectronic devices,<sup>16,17</sup> the Schottky barrier height is greater than  $E_g^{\text{InAs}} = 0.40 \text{ eV}$  by  $0.13 \text{ eV}$ .<sup>18</sup> Because of the large barrier, an inversion layer near the metal surface is formed, where in equilibrium the Fermi level is well above the conduction band edge of InAs and consequently the concentration of minority carriers (electrons) is much greater than the concentration of majority carriers (holes). By applying a significant positive bias voltage, the population inversion in InAs is created by injecting both electrons and holes into the active InAs region; electrons from the inversion layer are injected into the bulk of InAs and shift the electron quasi-Fermi level toward the conduction band, while p-InAs/p- $\text{AlAs}_{0.16}\text{Sb}_{0.84}$  heterojunction acts as an ohmic contact for holes, which penetrate easily from  $\text{AlAs}_{0.16}\text{Sb}_{0.84}$  into InAs and maintain the hole quasi-Fermi level at a fixed value of about  $2k_B T$  below the valence band edge (Figure 2). When the energy separation between quasi-Fermi level exceeds the SPP energy  $\hbar\omega$ , the stimulated emission into the SPP mode is initiated. Increasing

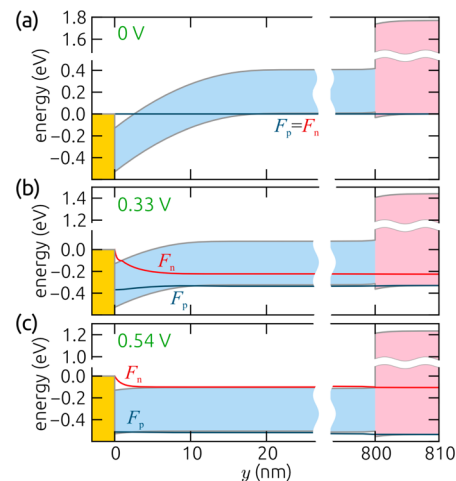


**Figure 2.** Energy band diagram of the Au/InAs/ $\text{AlAs}_{0.16}\text{Sb}_{0.84}$  single-heterostructure Schottky-barrier diode at zero (panel a), small forward (panel b), and high forward (panel c) biases;  $F_n$  and  $F_p$  are the quasi-Fermi levels for electrons and holes, respectively.

the bias voltage, it is eventually possible to completely compensate ohmic and radiation losses of the  $TM_{00}$  mode and, furthermore, amplify it.

In order to analyze the SPP amplification scheme, we have developed a self-consistent steady-state model describing the carrier behavior within the semiconductor that comprises the Poisson equation connecting the electrostatic potential and carrier density, the drift-diffusion current equations and the electron and hole continuity equations (see Supporting Information). The continuity equations cover generation and recombination of carriers involving three processes: non-radiative Auger recombination, spontaneous emission increased by a high density of guided modes (Purcell effect),<sup>19</sup> and stimulated emission. The later connects the electrical and optical properties of the structure and introduces in the equations the term describing SPP amplification. Providing the proper boundary conditions at the material interfaces and using the power flow distribution found in the eigenmode optical simulations (Figure 1b top panel), we have performed finite difference simulations using data for InAs and  $AlAs_{0.16}Sb_{0.84}$  adapted from refs 13 and 20 and obtain gain–current characteristics for various heights of the active InAs region (Figure 3). As can be seen, the propagation losses in the

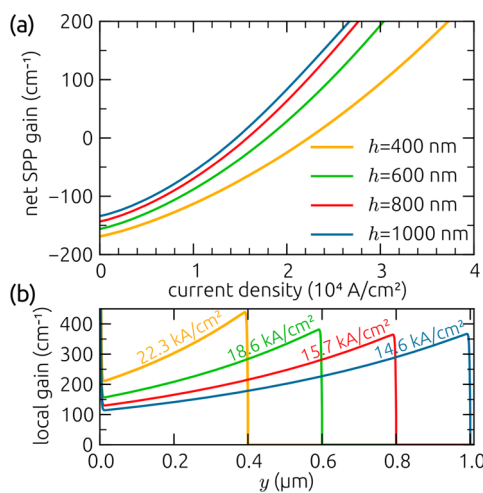


**Figure 3.** (a) Gain–current characteristic for the  $TM_{00}$  mode and (b) gain profile under full loss compensation at a small SPP power (less than 1  $\mu$ W) for different sizes of the active region and  $w = 350$  nm,  $H = 2$   $\mu$ m,  $\hbar\omega = 392.5$  meV. In graph (b), the corresponding current densities are shown next to each curve.

waveguide are fully compensated at pumping current densities in the range between 10 and 30 kA/cm<sup>2</sup>, above these currents the SPP is efficiently amplified. It should be emphasized that, in general, strongly confined plasmonic modes remarkably increase the spontaneous emission rate, which depletes the population inversion. However, at mid-infrared wavelengths, the Purcell factor near the metal surface is relatively small (in our case it does not exceed 3.5) and the spontaneous emission does not significantly suppress plasmonic gain.

The  $TM_{00}$  mode is well confined to the metal surface, its intensity penetration depth into the semiconductor is around 450 nm, therefore the active region height above this value is sufficient for efficient amplification of the plasmonic mode. The larger heights correspond to a better overlap between the mode and the gain profiles (Figure 3b), lower leakage into the substrate (reflected in the lower losses at zero pumping current

(Figure 3a), and consequently lower current densities required for full loss compensation. On the other hand, moderate heights of the active region ensure favorable discrimination between the amplification of plasmonic and photonic modes; the confinement of the  $TM_{00}$  mode to the active region is much higher than that of the  $TM_{01}$  and  $TE_{00}$  modes, therefore the plasmonic mode is efficiently amplified, while the propagation lengths of the photonic modes remain almost unchanged. Considering this trade-off, the height  $h = 0.8$   $\mu$ m appears to be close to the optimum.

Since the optical gain becomes lower at higher signal powers (the phenomenon known as gain saturation), the dependence of the net plasmonic gain on the signal SPP power is a very important characteristic of active plasmonic waveguides. The point is that each optical pulse must carry a certain amount of energy (a certain number of photons or SPP quanta) in order to be efficiently generated, modulated, transmitted, and detected. Assuming the pulse energy to be of the order of<sup>21</sup> 10–100 fJ and the required bit rate to be of about 100 Gbit/s, we easily obtain an average SPP power of the order of 1–10 mW. Accordingly, the amplification scheme should be capable of dealing with such high bit-rate data streams. As shown in Figure 4, the proposed structure can be used for

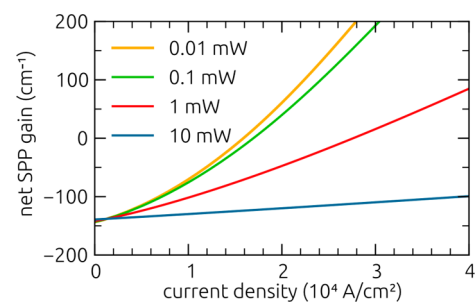


**Figure 4.** Gain–current characteristic for the  $TM_{00}$  mode of the T-shaped active waveguide ( $w = 350$  nm,  $H = 2$   $\mu$ m and  $h = 0.8$   $\mu$ m) at an SPP energy of 392.5 meV for different values of the SPP power.

lossless guiding of SPPs with a power of up to 3 mW at realistic current densities. In the case of an average SPP power of 1 mW, the efficiency, that is, the ratio of the current contributing to stimulated emission to the total current under full loss compensation is about 35%, which seems to be very high, especially in comparison with the efficiency of optically pumped active plasmonic devices.<sup>9,10</sup>

We proceed with the estimation of the performance of highly integrated large-scale plasmonic circuits enabled by the realization of electric pumping. The maximum single-channel bandwidth of the T-shaped waveguide is determined by the group-velocity dispersion (GVD)  $dv_g/d\omega$  of the guided mode (Figure 1c) and can be estimated as

$$B \approx \sqrt{\frac{1}{8\pi} \frac{v_g^2}{L \frac{dv_g}{d\omega}}} = \frac{B_0(\omega)}{\sqrt{L}} \quad (1)$$

where  $v_g$  is the group velocity,  $L$  is the waveguide length, and  $B_0(392.5$  meV) is calculated to be 3.3 Tbit-mm<sup>1/2</sup>/s for the waveguide parameters considered in this work (Figure 1b). Thus, the maximum bandwidth of a 1 mm long interconnect (typical length of on-chip global interconnects and upper estimate for on-chip local interconnects) is as high as 3.3 Tbit/s, that is, T-shaped waveguides are remarkably low-

dispersive and the actual bandwidth will be determined only by optical sources, modulators, detectors and the amplification bit-rate limit described above ( $\sim 100$  Gbit/s). In order to achieve this bit-rate limit, wavelength division multiplexing (WDM) or similar multichannel techniques can be used, allowing lower bit rate in each channel, while keeping the same total bit rate.

The integration density is essentially defined by the minimum waveguide separation (determined by the crosstalk, which is in turn related to the mode confinement) and the minimum waveguide bending radius. Usually, to characterize the mode confinement, a mode size is defined in various ways depending on the choice of mode profile analysis implemented.<sup>22,23</sup> In all such definitions, there is no selectivity between the mode height and the mode width, whereas all integrated circuits (both optical and electrical) are in fact planar, 2D dimensional circuits. It means that the mode height is not as important as the mode width, which actually determines the crosstalk and integration density. Furthermore, the estimation of the mode width gives only the first approximation to the crosstalk, since it essentially depends on the local distribution of the mode at any point. Therefore, instead of introducing the mode width, we consider the direct estimation of the crosstalk as the dependence of the coupling length  $L_{\text{coupl}}$  (the distance at which the mode initially launched in one waveguide is fully transferred to another one, placed parallel to it) on the separation distance between waveguides (Figure 5). In general, the interconnect length cannot exceed

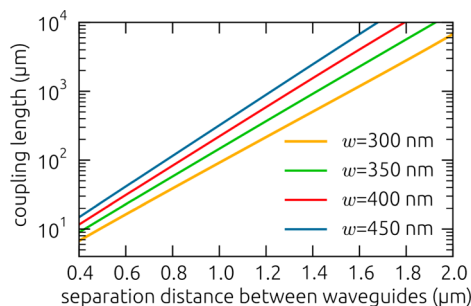


**Figure 5.** (a) Coupling length versus separation distance between the T-shaped active waveguides for different waveguide widths and  $h = 0.8 \mu\text{m}$ ,  $H = 2 \mu\text{m}$ ,  $\hbar\omega = 392.5$  meV.

$L_{\text{crit}} = \arcsin(1/4) \times L_{\text{coupl}}$ , corresponding to the case when 25% of the signal is transferred to the neighboring waveguide.<sup>24</sup> Consequently, by choosing the required length, we can find the smallest possible separation distance. Figure 5 shows that a separation of about  $1.5 \mu\text{m}$  is enough to design 1 mm long interconnects based on T-shaped active waveguides. Estimating the second factor, it has been found that the plasmonic mode can be transferred through a  $90^\circ$  bend having just  $1.5 \mu\text{m}$  radius with 95% efficiency (see Supporting Information), which ultimately defines a subwavelength size of all circuit components, such as splitters, ring resonators, and so forth.

To conclude, a novel approach for lossless guiding and amplification of an SPP mode upon electrical injection in a highly integrated optical circuitry has been demonstrated in mid-IR. A self-consistent electronic/photonic steady-state model, which in particular takes into account the plasmonic nature of the processes, has been developed and comprehensive numerical simulations based on this model have been performed. We have shown that the proposed amplification scheme provides lossless SPP propagation in  $\lambda/10$  wide

waveguides at moderate current densities ( $10\text{--}30$  kA/cm<sup>2</sup>). Finally, the developed approach leads to the realization of highly integrated large-scale hybrid electronic-plasmonic circuits and ultracompact coherent SPP sources (commonly regarded as nanolasers<sup>25</sup> or spasers)<sup>26</sup> integrated on a chip and easily coupled to plasmonic and photonic waveguides.

## ■ ASSOCIATED CONTENT

### 📄 Supporting Information

Self-consistent steady-state model for numerical simulations of the SPP amplification upon electrical injection, calculation of the dielectric function of gold, and simulation of the SPP transmission through a  $90^\circ$  bend. This material is available free of charge via the Internet at <http://pubs.acs.org>.

## ■ AUTHOR INFORMATION

### Corresponding Author

\*E-mail: feddu@mail.ru.

### Notes

The authors declare no competing financial interest.

## ■ ACKNOWLEDGMENTS

This work was supported in part by the Ministry of Education and Science of the Russian Federation (grants 07.514.11.4086, 14.740.11.1135), by the grant MK-334.2011.9 of the President of the Russian Federation, and by EPSRC (U.K.).

## ■ REFERENCES

- (1) Miller, D. A. B. *Appl. Opt.* **2010**, *49*, F59–F70.
- (2) Conway, J. A.; Sahni, S.; Szkopek, T. *Opt. Express* **2007**, *15*, 4474–4484.
- (3) Smit, M.; van der Tol, J.; Hill, M. *Laser Photonics Rev.* **2012**, *6*, 1.
- (4) Sarid, D. *Phys. Rev. Lett.* **1981**, *47*, 1927.
- (5) De Leon, L.; Berini, P. *Nat. Photonics* **2010**, *4*, 382.
- (6) Grandidier, J.; des Francs, G. C.; Massenet, S.; Bouhelier, A.; Markey, L.; Weeber, J.-C.; Finot, C.; Dereux, A. *Nano Lett.* **2009**, *9*, 2935.
- (7) Bolger, P. M.; Dickson, W.; Krasavin, A. V.; Liebscher, L.; Hickey, S. G.; Skryabin, D. V.; Zayats, A. V. *Opt. Lett.* **2010**, *35*, 1197–1199.
- (8) Gather, M. C.; Meerholz, K.; Danz, N.; Leosson, L. *Nat. Photonics* **2010**, *4*, 457.
- (9) Ma, R.-M.; Oulton, R. F.; Sorger, V. J.; Bartal, G.; Zhang, X. *Nat. Mater.* **2010**, *10*, 110.
- (10) Flynn, R. A.; Kim, C. S.; Vurgaftman, I.; Kim, M.; Meyer, J. R.; Mäkinen, A. J.; Bussmann, K.; Cheng, L.; Choa, F.-S.; Long, J. P. *Opt. Express* **2011**, *19*, 8954–8961.
- (11) Fang, A. W.; Park, H.; Cohen, O.; Jones, R.; Paniccia, M. J.; Bowers, J. E. *Opt. Express* **2006**, *14*, 9203–9210.
- (12) Fedyanin, D. Yu.; Arsenin, A. V. *Opt. Express* **2011**, *19*, 12524–12531.
- (13) Fedyanin, D. Yu. *Opt. Lett.* **2012**, *37*, 404–406.
- (14) *Springer Handbook of Electronic and Photonic Materials*; Kasap, S., Capper, P., Eds.; Springer: Berlin, 2006.
- (15) Tsou, Y.; Ichii, A.; Garmire, E. M. *IEEE J. Quantum Electron.* **1992**, *28*, 1261.
- (16) Melngailis, I.; Rediker, R. H. *J. Appl. Phys.* **1966**, *37*, 899.
- (17) Aydaraliev, M.; Zotova, N. V.; Karandashov, S. A.; Matveev, B. A.; Stus', N. M.; Talalakin, G. N. *Semicond. Sci. Technol.* **1993**, *8*, 1575.
- (18) Bhargava, S.; Blank, H.-R.; Narayanamurti, V.; Kroeme, H. *Appl. Phys. Lett.* **1997**, *70*, 759.
- (19) Iwase, H.; Englund, D.; Vučković, J. *Opt. Express* **2010**, *18*, 16546–16560.
- (20) Adachi, S. *Properties of Group-IV, III-V and II-VI Semiconductors*; Wiley: New York, 2005.
- (21) Miller, D. A. B. *Proc. IEEE* **2009**, *97*, 1166–1185.

- (22) Oulton, R. F.; Bartal, G.; Pile, D. F. P.; Zhang, X. *New J. Phys.* **2008**, *10*, 105018.
- (23) Krasavin, A. V.; Zayats, A. V. *Opt. Express* **2010**, *18*, 11791–11799.
- (24) International Technology Roadmap for Semiconductors, 2009 ed., Interconnect, [http://www.itrs.net/Links/2009ITRS/2009Chapters\\_2009Tables/2009\\_Interconnect.pdf](http://www.itrs.net/Links/2009ITRS/2009Chapters_2009Tables/2009_Interconnect.pdf).
- (25) Berini, P.; De Leon, I. *Nat. Photonics* **2012**, *6*, 16.
- (26) Stockman, M. I. *Opt. Express* **2011**, *19*, 22029–22106.